Progress in Physics of Applied Materials 3 (2023) 83–103

Semnan University

Progress in Physics of Applied Materials

journal homepage: https://ppam.semnan.ac.ir/

Chitosan – Graphite – Maghemite – a Flexible, Superparamagnetic Nanocomposite Comprising of Microcapacitors

A. Saravanan[a], R. P. Ramasamy[b]*

[a]*Department of Physics, Bharath Institute of Higher education and Research, Chennai – 600 073, INDIA.*

[b]*Department of Physics, CEG Campus, Anna University, Chennai – 600 025, INDIA.*

ARTICLE INFO

Article history:
Received: 30 August 2023
Revised: 11 October 2023
Accepted: 16 October 2023

Keywords:
Chitosan;
graphite;
maghemite nanoparticles;
Superparamagnetism

ABSTRACT

In this work, an eco-friendly "green" nanocomposite of chitosan containing graphite and maghemite (γ-Fe_2O_3) nanoparticles were prepared by solution casting method. The effect of γ-Fe_2O_3 nanoparticles on structural, electric and dielectric properties of Chitosan-graphite (Cs-graphite) composites was investigated. The dielectric constant of Cs-graphite composites increased with incorporation of γ-Fe_2O_3 nanoparticles. Among the composites Cs-20% graphite - 20% γ-Fe_2O_3 has dielectric constant of ~16.5 at 1 MHz at room temperature. With increase in temperature the dielectric constant varied significantly. The conductivity of Cs-graphite is enhanced by one order of magnitude with addition of γ-Fe_2O_3 nanoparticles, and the value is found to be 5.7×10^{-6} S/cm. Various parameters such as dielectric constant, dielectric loss, electric modulus, conductivity, activation energy were analyzed. Magnetic measurement of γ-Fe_2O_3 nanoparticles and the PNCs showed superparamagnetic behaviour. A model is proposed to explain the observed dielectric behavior of polymer nanocomposites (PNCs). The formation of microcapacitors by incorporation of maghemite nanoparticles between graphite is proposed.

1. Introduction

The increasing demand for environmentally friendly materials has attracted great interest. Recently, researchers are actively involved in the development of natural polymers for energy storage applications due to their remarkable cycle stability and dielectric properties [1]. These bio polymeric materials act as potential alternative for synthetic and petroleum based polymers. Many natural polymers such as cellulose [2], starch [3] and chitosan [4] have been extensively investigated for energy storage and conversion applications. Chitosan, a biopolymer derived from the chitin is the second most abundant organic material on earth after cellulose. Chitin is found in crustacean cells, insect exoskeletons and fungus cell walls [5]. Chitosan is copolymer composed of N-acetyl-D-glucosamine and D-glucosamine residue, where the two types of repeating units are linked by (1→4)-β-glycosidic bonds. It has significant properties such as film & gel forming capability, high adsorption capacity, biodegradability and biocompatibility [6]. The main advantage of chitosan is that it can be made easily in the form of gel, films, beads, nanoparticles, capsules and tablets [7]. It also has a remarkable capability of reducing gold and silver metal ions ($HAucl_4$ and $AgNO_3$) into nanoparticles with low particle size distribution [8-9]. A monomer of chitosan consists of two hydroxyl and one amine functional groups which have lone pair electrons that are suitable for the preparation of solid polymer electrolyte [10-11]. It is also used as a proton exchange membrane for fuel cells [12], an effective binder material for graphite anode in Li-ion batteries [13] and for optical sensors [14].

In this research we studied the dielectric properties of chitosan, graphite and γ-Fe_2O_3 nanoparticles. Graphite and γ-Fe_2O_3 are selected as the conductive filler because of its low cost, high availability and favourable biodegradable properties. Graphite has good electrical and thermal

* Corresponding author. Tel.: 08608762302
E-mail address: perumal.ramasamy@gmail.com

DOI: 10.22075/ppam.2023.31598.1063

conductivity, excellent mechanical strength, thermal and chemical stability [15-16]. More importantly, it has large aspect ratio and unique layered structure with nanoscale thickness, which give advantages in the formation of a large number of parallel board microcapacitors with low filler loading [17-18]. Maghemite is one of the important oxides of iron. It is one of the low costs, naturally abundant and environmentally friendly metal oxides. When its size is reduced below certain critical limit, it transforms from multi domain state to single domain state and shows superparamagnetic behaviour [19]. This superparamagnetic behaviour of the nanoparticles has wide applications in the field of biomedicine, such as magnetic separation, drug delivery, magnetic resonance imaging (MRI) and hyperthermia [20]. Recently, the superparamagnetic iron oxide nanoparticles have been used for high performance supercapacitor electrode applications [21]. The high active surface area (because of reduction in the particle size) of the nanoparticles can drastically improve the charge storage capacity. Carbon based nanocomposites with well dispersed γ-Fe_2O_3 nanoparticles have been used for high performance supercapcitor [22]. Therefore, the incorporation of γ-Fe_2O_3 nanoparticles in to the Cs-graphite can have important role as energy storage material. Understanding the charge transport in these polymer nanocomposites is important as it can help in the development of new energy storage materials [23]. The frequency and temperature dependent dielectric measurements are both sensitive to the motion of charged species and dipoles in these nanocomposites. Hence, in this research the electric and dielectric properties of the chitosan-graphite-γ-Fe_2O_3 nanocomposites are studied. In the present work, green nanocomposite of chitosan containing γ-Fe_2O_3 nanoparticles and graphite have been prepared by solution casting method. The surface morphology, electric and dielectric properties of the nanocomposites have been investigated by using various analytical methods. A model is proposed.

2. Experimental Procedure

Chitosan powder (99.9% purity), acetic acid (99.9% purity) and graphite nano powder (98% purity) were all purchased from SRL Pvt. Ltd, Mumbai, India. Iron nitrate nanohydrate ($FeNO_3.9H_2O$ - 98% purity) and ammonium hydroxide solution were purchased from Merck Specialities Pvt Ltd, Mumbai, India. The Ferrous sulphate heptahydrate ($FeSO_4.7H_2O$- 98% purity) was purchased from RFCL Limited, New Delhi, India. Deionised water was used throughout the experiments. All the reagents used in the experiment were of analytical grade and used as received without further purification.

2.1. Preparation of γ-Fe_2O_3 nanoparticles

Iron oxide nanoparticles were prepared by a co-precipitation method consisting of a stoichiometric mixture of $FeSO_4.7H_2O$ (0.1M) and $FeNO_3.9H_2O$ (0.2M) in an aqueous solution [24-25]. The mixture was stirred for 30 minutes using magnetic stirrer in nitrogen atmosphere at room temperature to obtain homogeneous solution and 0.3M of NH_3OH solution was added to the mixture drop by drop until the formation of black precipitate. The precipitation was formed at a pH between 8 and 14. Formed black precipitate was collected and centrifuged five times by giving alternate wash with distilled water, acetone, and ethanol. Finally, the precursor was kept in oven at 100^{o}C for 12hr. The obtained black powder was sintered at 300^{o}C for 2hr to get light brown coloured γ-Fe_2O_3 nanoparticles.

2.2. Preparation of Chitosan-graphite nanocomposites

Chitosan solution was prepared by adding chitosan powder (1 wt %) to acetic acid solution (200 mL, 1.5 wt %). The mixture was stirred using magnetic stirrer and heated at 60°C for 30-45 min. A semi-transparent solution was obtained. Series of chitosan-graphite nanocomposites were prepared by adding appropriate amounts of graphite (10 and 20 wt %) into the chitosan solution and it was ultrasonicated for 30 min for complete dispersion of graphite into the chitosan solution. The mixture was poured into a petri dish for drying. Finally, the chitosan solution containing 10 and 20 wt % of graphite were labelled as Cs-10% graphite and Cs-20% graphite, respectively.

2.3. Preparation of Chitosan-graphite-γ-Fe_2O_3 nanocomposites

Appropriate amount maghemite nanoparticles (20 wt %) were added into each of the Chitosan - graphite solution having varying concentration of graphite (10-20wt %) and it was ultrasonicated for 30 min for complete dispersion of maghemite into the chitosan-graphite solution. The mixture was poured into a petri dish for drying. The obtained films were labelled as Cs-10%graphite-20%γ-Fe_2O_3 and Cs-20%graphite-20% γ-Fe_2O_3. The films were flexible.

2.4. Characterization

The crystallinity of the prepared samples was characterized by using Powder X-ray diffraction (XRD) technique using PANalytica X'pert pro X-ray diffractometer with Cu-Kα radiation (λ = 0.154060 nm) operated at 30 kV and 30 mA. FTIR spectra of the samples were collected by using Bruker Alpha FTIR spectrometer (Bruker Optics GmbH, Germany). Measurements were recorded in the MIR spectral range from 500-4000 cm^{-1} with a spectral resolution of 2 cm^{-1} using ATR mode. The Raman spectra were obtained by using Confocal scanning spectrometer (Renishaw InVIA) with 532 nm excitation source in the range from 100cm^{-1} to 3000 cm^{-1} at room temperature. Morphological and structural information was obtained using high resolution scanning electron microscopy (Hitachi S6600). The impedance properties were measured using Wayne Kerr impedance analyzer (Model:6500B) in the frequency range of 20 Hz to 1 MHz and in the temperature range of 303K to 423K at ac electric signal of 1 volt. The samples were used in the form of circular films with a diameter of 1cm and thickness of 80-110 μm. The samples were kept in between two gold coated circular Cu

plate electrodes for measurements. Magnetic measurements were carried out by using Superconducting Quantum Interference Device–Vibrating sample magnetometer (SQUID - VSM) (Quantum Design, USA) at room temperature in the field range from -70 kOe to +70 kOe.

3. Results and discussion

3.1. Structural studies

The optical images of the chitosan film and the PNCs are shown in Figure 1A. It is observed that the chitosan film looks transparent and it became gray in colour when 20% γ-Fe_2O_3 nanoparticles was added to it. When graphite was added to the chitosan, it became less transparent when compared to pure chitosan. Cs-graphite containing γ-Fe_2O_3 nanoparticles looked similar to Cs-graphite composites. Figure 1B shows the optical image of chitosan and Cs-graphite containing γ-Fe_2O_3 nanoparticles. The magnetic nature of the nanocomposite is also shown.

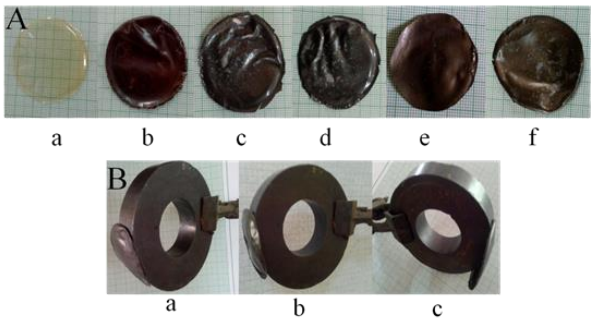

Fig. 1. A) Optical images of (a) chitosan film, (b) Cs-20% γ-Fe_2O_3, (c) Cs-10% graphite, (d) Cs-20% graphite, (e) Cs-10% graphite-20%γ-Fe_2O_3 and (f) Cs-20% graphite-20%γ-Fe_2O_3; B) attracted by magnet for (a) Cs-20% γ-Fe_2O_3, (b) Cs-10% graphite-20% γ-Fe_2O_3 and (c) Cs-20% graphite- 20% γ-Fe_2O_3.

3.2. X-ray diffraction studies

Fig. 2 (i) shows the XRD pattern of a) chitosan, b) γ-Fe_2O_3 nanoparticles and c) Cs-20% γ-Fe_2O_3. It is well know that chitosan is a semi crystalline polymer having both amorphous and crystalline structure. It shows sharp peaks at 2θ = 11°, 18° and broad peak at 24°. The former two peaks indicate the hydrated crystalline phase, while the latter broad peak corresponds to the existence of an amorphous phase [26]. The diffraction pattern of γ-Fe_2O_3 shows peaks at 2θ = 30.2°, 36.2°, 43.4°, 53.74°, 57.5° and 63° which correspond to Bragg's reflections of (220), (311), (400), (422), (511) and (440) diffraction planes, respectively. All the peaks were indexed to the typical cubic spinel structure of maghemite (JCPDS 39-1346) and no impurity phase was observed [27]. The average crystallite size, D (nm), of the γ-Fe_2O_3 nanoparticles was calculated from predominant (311) peak by using Debye-scherrer equation.

$$D = \frac{k\lambda}{\beta \cos\theta} \quad (1)$$

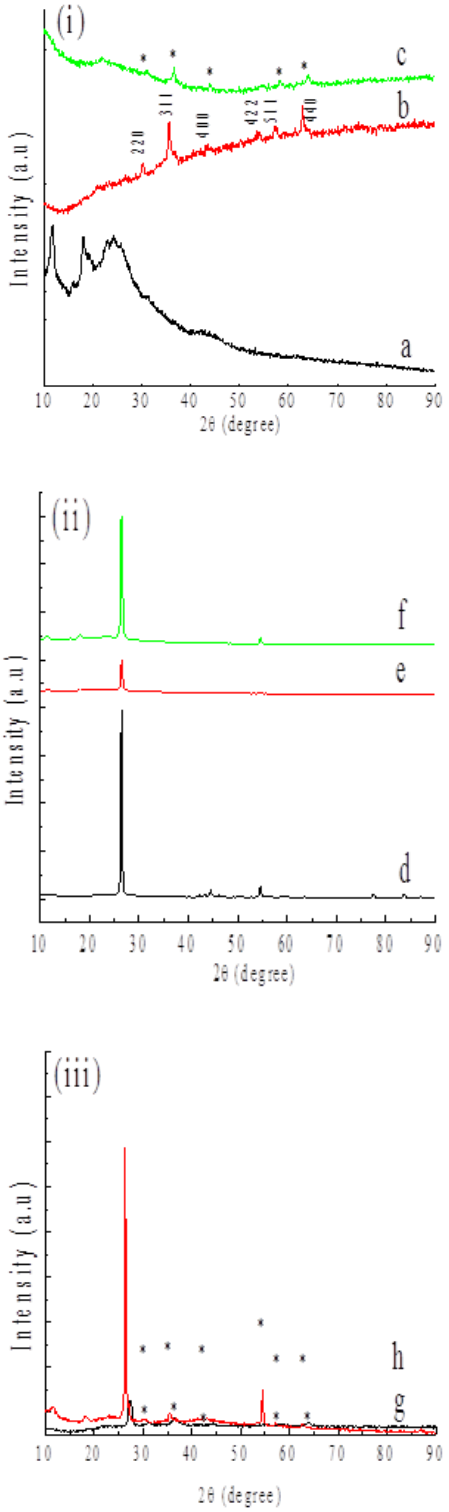

Fig. 2. (i) XRD pattern of a) Chitosan film b) γ-Fe_2O_3 Nps and c) Cs-20% γ-Fe_2O_3; (ii) d) graphite, e) Cs-10% graphite, f) Cs-20% graphite and (iii) g) Cs-10% graphite-20% γ-Fe_2O_3, h) Cs-20% graphite-20% γ-Fe_2O_3.

Where k is shape factor (k = 0.9 for Cu Kα radiation), λ (nm) is the wave length (0.15405 nm for Cu Kα radiation), β is the peak width at half maximum (rad) and θ is the diffraction angle. The average crystallite size of the γ-Fe_2O_3 nanoparticles is found to be ~ 14 nm. The XRD pattern for Cs-20% γ-Fe_2O_3 shows presence of small peak of γ-Fe_2O_3 peak (as indicated by star symbol) which confirm the

incorporation of γ-Fe_2O_3 nanoparticles into the chitosan matrix. This result indicates that chitosan does not lead to change in the structure of the maghemite nanoparticles. The XRD pattern of graphite powder [Figure 2(ii-d)] shows sharp and strong crystalline peak around $2\theta = 26.4^{\circ}$. This peak indicates layered structure of graphite which correspond to d_{002} diffraction plane [28]. The XRD pattern of chitosan containing 10% and 20% of graphite [Figure 2 (ii e-f)] shows presence of graphite peak at $2\theta = 26.4$. Also, the predominant peak of graphite is not affected when it is incorporated into the chitosan. The predominant peak intensity is increased by increase in graphite concentration from 10 to 20 wt%. The XRD pattern of Cs-20% γ-Fe_2O_3 containing 10 to 20 wt% of graphite [Figure 2(iii g-h)] shows the presence of both graphite and γ-Fe_2O_3 diffraction peaks. The graphite peak position in the Cs-graphite-γ-Fe_2O_3 is not affected by introduction of γ-Fe_2O_3 nanoparticles. The γ-Fe_2O_3 peaks are indicated by star symbol in the XRD patterns. The predominant graphite peak has high intensity compared to γ-Fe_2O_3 peak in the composites. It is also observed that the intensity of peak for graphite is increased by increasing its concentrations of graphite from 10 to 20 wt%. The XRD measurements confirms the incorporation of graphite and γ-Fe_2O_3 nanoparticles into the chitosan matrix. To understand the modifications in the crystallinity of chitosan due to the presence of graphite and γ-Fe_2O_3 nanoparticles the following expressions were used [29].

$$\text{Cr } I_{020} = (I_{020} - I_{am})/I_{020} \times 100 \quad (2)$$

$$\text{Cr } I_{110} = (I_{110} - I_{am})/I_{020} \times 100 \quad (3)$$

Here I_{am} is the intensity of amorphous diffraction at~ 2θ equal to 12°, I_{020} is the maximum intensity of the crystalline peak due to (020) lattice diffraction, and I_{110} is the highest intensity of the crystalline peak by (110) lattice diffraction planes. $I_{020\ is}$ observed at 11.6° and I 110 is observed at 18°. The values for Cr I_{020} for chitosan, Cs-10% graphite and Cs-20% graphite and were 40%, 54% and 72% respectively, indicating that the crystallinity of chitosan increased with incorporation of graphite in it. The values for Cr I_{110} for chitosan, Cs-10% graphite and Cs-20% graphite and were 28%, 64% and 80% respectively, indicating that the crystallinity of chitosan increased with incorporation of graphite in it. With incorporation of γ-Fe_2O_3 the Cr I_{020} for Cs-20%γ-Fe_2O_3, Cs-10%graphite-20%γ-Fe_2O_3 and Cs-20%graphite-20% γ-Fe_2O_3 were found to be 14%, 21% and 32% respectively. Hence the incorporation of γ-Fe_2O_3 decreases the crystallinity of chitosan. Hence while graphite increases the crystallinity of chitosan, γ-Fe_2O_3 decreases it. With incorporation of 20% γ-Fe_2O_3 the peak corresponding to I_{110} was diminished and its intensity became lesser than that of the intensity for the amorphous diffraction at 12° and hence the crystallinity could not be found for (110).

3.3. FTIR Analysis

ATR-FTIR measurement of chitosan film, graphite, γ-Fe_2O_3 nanoparticles and the PNCs are shown in Figure 3. Chitosan film shows characteristic peaks at 1540 cm^{-1} and 1404 cm^{-1} corresponding to amide II group and bending vibration of CH_3 respectively. The peak corresponding to 1147 cm^{-1} represents asymmetric stretching of the C–O–C bridge. The peaks at 1057 cm^{-1} and 1012 cm^{-1} indicate the saccharine structure of chitosan molecules [30]. For graphite, strong peaks at 3426 cm^{-1} and 1386 cm^{-1} are observed indicating the presence of OH groups attached to graphite. The peaks at 2922 cm^{-1} and 2853 cm^{-1} represents the stretching vibration of C-H bonds (29-31). The bands at 1634 cm^{-1} and 1575 cm^{-1} are attributed to the vibration of C=C bond and amide II group, respectively. The peak observed at 1458 cm^{-1} is related to the bending vibration of C-H groups and the peak at 1123 cm^{-1} is assigned to the C-H deformation. The FTIR spectrum of γ-Fe_2O_3 shows the absorption bands at 627 cm^{-1} and 590 cm^{-1} corresponding to the metal oxygen [υ (Fe-O)] deformations in tetrahedral and octahedral sites (31-36). In FTIR spectrum of Cs-20% γ-Fe_2O_3, compared with spectrum of chitosan film, the 1540 cm^{-1} band of amide II, the 1404 cm^{-1} band of bending vibration of CH_3 and the 1147 cm^{-1} band of asymmetric stretching of the C–O–C bridge were shifted to 1527 cm^{-1}, 1391 cm^{-1} and 1145 cm^{-1} respectively. This shift of the peak indicates that γ-Fe_2O_3 nanoparticles attached to chitosan. Similar kind of band shift has been observed for the chitosan containing iron oxide nanoparticles (37). The FTIR spectrum of chitosan containing graphite shows peaks with less intensity. The main changes in the absorbance bands of chitosan due to addition of fillers (γ-Fe_2O_3 nanoparticles and graphite) is described as follows: The amide II band of Cs-10% graphite, Cs-10%graphite-20%γ-Fe_2O_3, Cs-20% graphite and Cs-20%graphite-20%γ-Fe_2O_3 were observed at 1508, 1517, 1530 and 1529 cm^{-1}, respectively. Similarly, the bending vibration of CH_3 for Cs-10% graphite, Cs-10%graphite-20%γ-Fe_2O_3, Cs-20% graphite and Cs-20%graphite-20%γ-Fe_2O_3 were observed at 1402, 1386, 1396 and 1393 cm^{-1}, respectively. The saccharine structure band of Cs-10% graphite, Cs-10%graphite-20%γ-Fe_2O_3, Cs-20% graphite and Cs-20%graphite-20%γ-Fe_2O_3 were observed at 1008, 1005, 1010 and 1005 cm^{-1}, respectively. The lower wave number shift in the position of the absorbance peaks indicates that the amide II band, bending vibration of CH_3 and the saccharine structure of chitosan film have been affected due to the addition of γ- Fe_2O_3 nanoparticles and graphite. To further understand the interactions in the nanocomposites, Raman measurement was done and the results are as under.

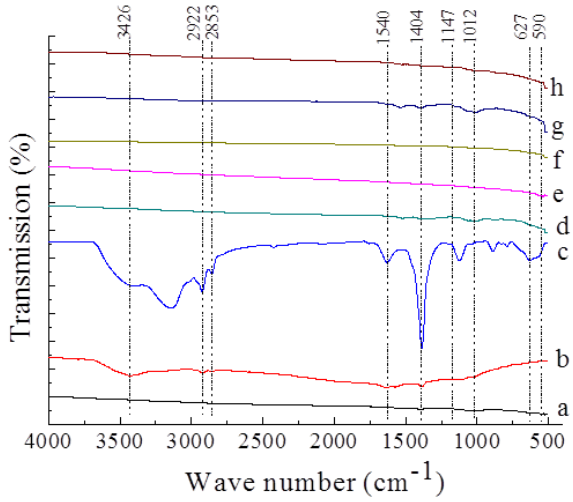

Fig. 3. FTIR spectra for a) chitosan film b) graphite, c) γ-Fe_2O_3 Nps, d) Cs-20% γ-Fe_2O_3, e) Cs-10% graphite, f) Cs-10% graphite-20% γ-Fe_2O_3, g) Cs-20% graphite and h) Cs-20% graphite-20% γ-Fe_2O_3.

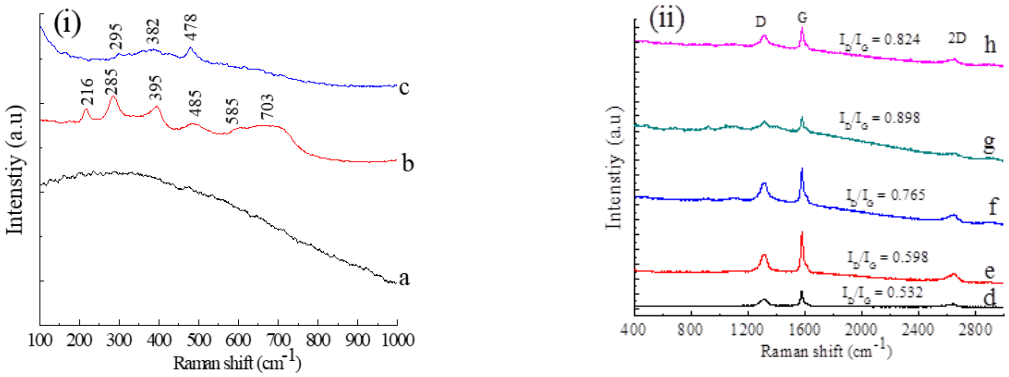

Fig.4. (i) Raman spectra of a) Chitosan film b) γ-Fe_2O_3 Nps and c) Cs-20% γ-Fe_2O_3; (ii) d) graphite, e) Cs-10% graphite, f) Cs-20% graphite, g) Cs-10% graphite-20% γ-Fe_2O_3, h) Cs-20% graphite-20% γ-Fe_2O_3.

Table 1. Raman shift and ID/IG ratio of graphite and it's PNCs.

S. No	Sample	D band	G band	2D band	I_D/I_G
1.	Graphite	1315	1578	2639	0.532
2.	Cs-10%graphite	1315	1578	2652	0.598
3.	Cs-20%graphite	1315	1578	2645	0.765
4.	Cs-10%graphite-20%γ-Fe_2O_3	1315	1578	2639	0.898
5.	Cs-20%graphite-20%γ-Fe_2O_3	1315	1578	2652	0.824

3.4. Raman spectroscopy analysis

Raman spectroscopy is an important tool to understand the composite functional groups and their interactions within the matrix. Figure 4 (i) shows the Raman spectra of a) chitosan, b) γ-Fe_2O_3 Np's and c) Cs-20% γ-Fe_2O_3. Chitosan film does not show any peak. The γ-Fe_2O_3 nanoparticles shows fundamental Raman scattering peaks at 216, 285, 395, 485, 585 and 703 cm^{-1}, corresponding to the characteristic band of maghemite phase of the iron oxide nanoparticles [38]. The main peak for maghemite peak is observed at 703 cm^{-1} [39]. The Raman spectrum of Cs-20% γ-Fe_2O_3 shows the peaks at 295, 382 and 478 cm^{-1}, which indicates the incorporation of γ - Fe_2O_3 nanoparticles into the chitosan matrix. The Raman spectrum of the graphite [Figure 3(ii-d)] shows three strong peaks centred at 1348 cm^{-1}, 1573 cm^{-1} and 2650 cm^{-1}, respectively which corresponds to the D, G and 2D bands of graphite. The D band at 1348 cm^{-1} is assigned to the vibrations of sp^3 carbon atoms of disordered graphite and the G band at 1573 cm^{-1} is related to the plane vibration of sp^2 carbon

atoms in a 2D hexagonal lattice [40]. The 2D band is the second harmonic (or overtone) of the D-band. The shape and intensity of 2D band indicates the layered structures of graphite rather than single layer graphene [41]. With addition of 20% γ-Fe_2O_3 into the matrix, the raman intensity of graphite bands decreased as shown in Figure 3 (ii-g,h). The Raman shift and the corresponding I_D/I_G intensity ratio values are listed in the table.1. The intensity of the D and G band represents the concentration of disordered carbon and graphitized carbon present in the sample, respectively [42-43]. The relative intensity ratio of the D band to G band (I_D/I_G ratio) is proportional to the content of defect sites in graphite and it also indicates the edge smoothness and the edge structures of the carbon materials [44-46]. In the present study, the I_D/I_G ratio of graphite, Cs-10%graphite and Cs-20% graphite was found to be 0.532, 0.598 and 0.765, respectively. Also, the I_D/I_G ratio of Cs-10%graphite-20% γ-Fe_2O and Cs-20%graphite-20% γ-Fe_2O was observed to be 0.898 and 0.824, respectively. The composites of Cs-graphite-γ-Fe_2O_3 have a higher I_D/I_G ratio then that of Cs-graphite and graphite, which suggest that more defects were introduced in graphite due to its interactions between the chitosan and γ-Fe_2O_3 nanoparticles.

3.5. FE-SEM: Morphology and Microstructure studies

The surface morphologies and microstructures of the chitosan and PNCs were studied by FE-SEM (Figure 5). Chitosan [Figure 5a] shows smooth surface with lots of pores. Addition of γ-Fe_2O_3 into chitosan made the sample's surface rough [Figure 5b]. Further addition of graphite [Figure 5c and 5d] resulted in plate like structure due to graphite. The incorporation of γ-Fe_2O_3 in graphite containing nanocomposite could result in modifications in the dielectric properties of the nanocomposites. The dielectric characteristics were studied and the results are as under.

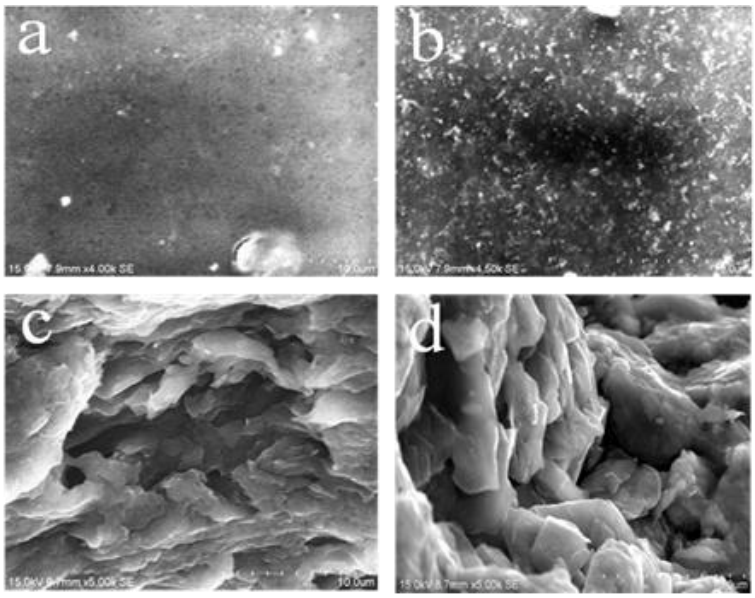

Fig.5. FE-SEM images of a) Chitosan, b) Cs-20% γ- Fe_2O_3, c) Cs-20% graphite and d) Cs-20% graphite-20% γ- Fe_2O_3 (Scale bar: 10 μm).

3.6. Dielectric measurement studies

Dielectric measurement has been used to obtain various parameters such as dielectric constant (ε'), dielectric loss (ε''), electric modulus (M'&M''), electrical conductivity (σ') and dissipation factor (D). When the material is subjected to the electric field, the interaction between the material and the electric field is described by the complex permittivity (ε* = ε'– ε''). The real part of the permittivity (ε') represents the energy stored in the material and the imaginary part (ε'') is associated with the energy loss during the polarization [47-48]. The dielectric constant (ε') was calculated by using the equation,

$$\varepsilon' = CL/\varepsilon_o A \quad (4)$$

Here, C is the capacitance of the sample, L is the thickness of the sample, A is the electrolyte–electrode contact area and ε_o is the permittivity of free space. The dielectric loss (ε'') was calculated from ε' by using following expression [49].

$$\varepsilon_{cal}'' = -(\pi/2)(\partial(\varepsilon')/\partial \ln(\omega)) \quad (5)$$

This method is more convenient to observe relaxation frequency due to its peak sharpening [50]. The electric modulus (M*) is defined as the reciprocal of the dielectric permittivity (ε*) and represented by,

$$M^* = 1/\varepsilon^* = M' + iM'' \quad (6)$$

M' and M'' were obtained from the dielectric constant (ε') and dielectric loss (ε'') as follows.

$$M' = \varepsilon'/[\varepsilon'^2 + \varepsilon''^2] \quad (7)$$
$$M'' = \varepsilon''/[\varepsilon'^2 + \varepsilon''^2] \quad (8)$$

The complex dielectric permittivity [$\varepsilon^*(\omega) = \varepsilon'(\omega) - i\varepsilon''(\omega)$] and complex electrical conductivity [$\sigma^*(\omega) = \sigma'(\omega) + i\sigma''(\omega)$] are related to each other by the equation, $\sigma^*(\omega) = i\omega\varepsilon_0\varepsilon^*(\omega)$. The electrical conductivity (σ') was calculated by using the formula,

$$\sigma' = L / RA \quad (9)$$

Where, L is the thickness of the sample, R is the resistance of the sample and A is the electrolyte–electrode contact area. The Dissipation factor (D) is defined as the ratio of energy loss to energy stored in the material ($\varepsilon''/\varepsilon'$). It decides the suitability of a dielectric material for microwave applications.

3.6.1. Frequency dependence of dielectric constant (ε')

Fig. 6 shows the real part of the permittivity plotted as a function of frequency for the PNCs in the temperature range 303 - 423K. It is observed all the sample have high value of ε' at low frequency and it is decreased with an increase in frequency. This is in accordance with reported findings [51-52]. It is also observed that the ε' increased with increase in temperature [53]. The sharp increase of ε' at low frequency is due to electrode polarization [54]. The ε' of chitosan [Figure 6a] decreases with increase in frequency and it increases with an increase in temperature up to 363K. Above 363K, it decreases with further increasing of temperature. When 20wt% γ-Fe_2O_3 nanoparticles were added into the chitosan, the ε' enhanced significantly. The ε' of Cs-20% γ-Fe_2O_3 [Figure 6b] decreases with increase in frequency and it increases gradually with increase of temperature up to 363K. Above 363K, it decreased with increase of temperature. The ε' of chitosan is enhanced with addition of graphite. The ε' of Cs-10% graphite [Figure 6c] decreased with increase in frequency and it is gradually increased with increase in temperature up to 423K. The $\varepsilon'$of Cs-10% graphite-20% γ-Fe_2O_3 [Figure 6d] decreased with an increase in frequency and it gradually increased with temperature up to 383K, after that it is decreased with further increase of temperature. The sudden decrease of ε' is due to the presence of γ-Fe_2O_3 nanoparticles in the Cs-graphite composites. When graphite concentration is increased from 10 to 20%, it's ε' value is enhanced. The $\varepsilon'$of Cs-20% [Figure 6e] graphite shows decreasing trend with increase in frequency and it slowly increased with increase in temperature up to 383K, after that it is decreased with further increase of temperature up to 423K. The ε' of Cs-20% graphite-20% γ-Fe_2O_3 [Figure 6f] is also shows decreasing trend with increase in frequency and it is slowly increased with increase in temperature up to 383K, after that the ε' decreased with further increase of temperature up to 423K. The observed dielectric constant (ε') values of chitosan and its PNCs measured at 1 kHz and 1 MHz at 303,323, 373 and 423K are listed in the table 2. It is observed from the table, that the dielectric constant of Cs-10% graphite is found to be ~ 6.0 at room temperature and it increased to ~ 12.5 with incorporation of 20 wt% of γ-Fe_2O_3 nanoparticles in it. When graphite concentration is increased from 10 to 20wt%, the dielectric constant is found to be ~ 6.6 and it is further increased to ~ 16.5 with addition of 20 wt% of γ-Fe_2O_3 nanoparticles. It is 14 times higher than that of pure chitosan matrix. It is further observed that the dielectric constant of Cs-graphite and Cs-graphite -γ-Fe_2O_3 composites increases with an increase in temperature. This is due to dependence of dielectric constant upon temperature [55]. The dielectric constant of composites containing graphite and maghemite is larger than the addition of dielectric constant of the composites without both maghemite and graphite. This indicates that maghemite might get trapped between two graphites and create microcapacitors with higher capacitance.

Table 2. The ε' values of chitosan and its PNCs measured at different frequency.

S. No	Sample	303K		323K		373K		423K	
	Frequency	**1kHz**	**1MHz**	**1kHz**	**1MHz**	**1kHz**	**1MHz**	**1kHz**	**1MHz**
1.	Chitosan	3.767	1.178	4.941	1.224	4.742	1.273	2.489	1.216
2.	Cs-20%γ-Fe_2O_3	7.815	2.244	11.243	2.367	5.544	2.450	5.373	2.427
3.	Cs-10%graphite	14.292	6.036	19.605	6.439	85.653	7.379	211.78	10.396
4.	Cs-10%graphite-20%γ-Fe_2O_3	64.139	12.526	99.86	14.467	1524.7	26.716	608.06	26.211
5.	Cs-20%graphite	34.736	6.644	47.755	7.131	311.80	8.913	271.51	10.679
5.	Cs-20%graphite-20%γ-Fe_2O_3	257.76	16.561	376.24	19.392	6300.7	36.180	1954.1	37.718

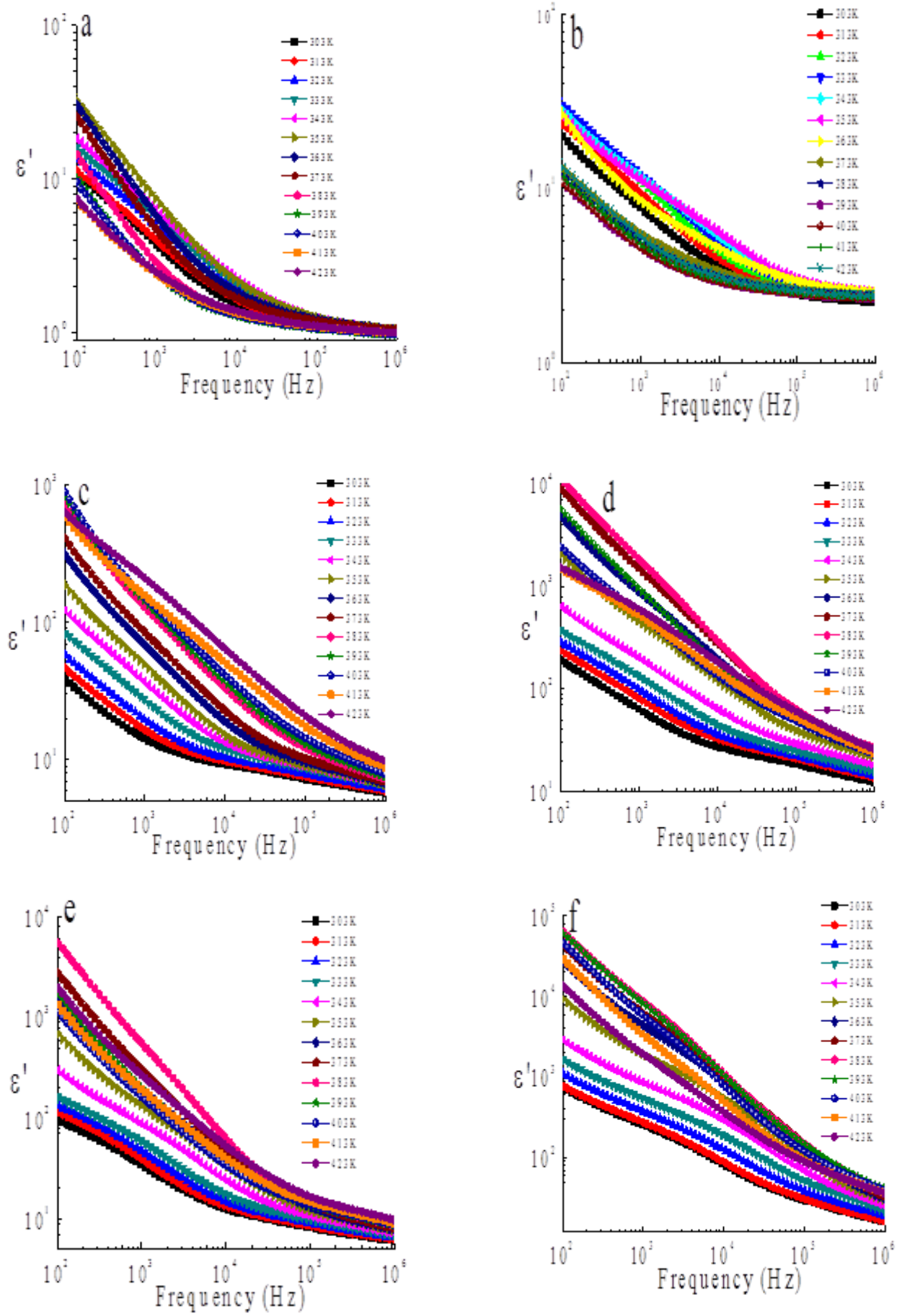

Fig. 6. Frequency dependent variation of dielectric constant (ε') at various temperature for a) Chitosan, b) Cs-20% γ-Fe2O3, c) Cs-10% graphite, d) Cs-10% graphite-20% γ-Fe2O3, e) Cs-20% graphite and f) Cs-20% graphite-20% γ-Fe2O3.

3.6.2. Frequency dependence of ε''

The dependence of dielectric loss on the frequency at different temperature for chitosan and the PNCs is shown in Figure 7. The relaxations in chitosan and the composites were observed in the two different temperature region: i) 303-363K and (ii) 403K-423K. Chitosan [Figure7a] shows relaxation at low temperature (303-363K) between ~692 Hz and ~7878 Hz and relaxation at high temperature (403-423K) between ~311 Hz and ~1775 Hz. When 20wt% of γ-Fe_2O_3 nanoparticles were added into the chitosan, the relaxation peaks shifted to high frequency. Cs-20%γ-Fe_2O_3 [Figure 7b] shows relaxation at low temperature (303-363K) between ~2001 Hz and ~26,606 Hz and relaxation at high temperature (403-423K) in between ~1,74,769 Hz and ~2,90,477 Hz. When 10wt% graphite was added into the chitosan, it shows new relaxation in addition with relaxation observed for chitosan. Cs-10% graphite [Figure 7c] shows the relaxation at low temperature (303-363K) between ~113 Hz and ~4,551 Hz and relaxation at high temperature (403-423K) in between ~25,950 Hz and ~ 68,191 Hz. An additional new relaxation was observed in between ~66,508 Hz and ~ 86,821 Hz in the temperature range of 303-323K. When 20wt% of γ-Fe_2O_3 nanoparticles were added into the Cs-10% graphite, the relaxation peaks were shifted to high frequency. Cs-10%graphite-20%γ-Fe_2O_3 [Figure 7d] shows the relaxation at low temperature (303-363K) in between ~1042 Hz and ~16,008 Hz and relaxation at high temperature (403-423K) in between ~2,156 and ~2,612 Hz. An additional relaxation was observed in between ~1,47,542 Hz and ~ 2,07,021 Hz in the temperature range of 303-323K. When increasing the graphite concentration from 10 to 20 wt%, the high frequency relaxation observed for Cs-10% graphite disappeared. The Cs-20% graphite [Figure 7e] shows the relaxation at low temperature (303-363K) between ~ 628 Hz and ~15,227 Hz and relaxation at high temperature (403-423K) between ~2,430 Hz and ~ 4,551 Hz. When 20wt% of γ-Fe_2O_3 nanoparticles is added into the Cs-20% graphite, the relaxation peaks were shifted to high frequency side. Cs-20%graphite-20%γ-Fe_2O_3 [Figure 7f] shows the relaxation at low temperature (303-363K) between ~7038 Hz and ~26,606 Hz and relaxation at high temperature (403-423K) between ~8,836 Hz and ~10,614 Hz.

3.6.3. Frequency dependence of M' and M''

Electric modulus formalism is mainly used to analyze the electrical relaxation process. It is defined as the reciprocal of complex permittivity [56-57]. The real (M') and imaginary (M'') parts of electric modulus were calculated by using equations 5 and 6 and is shown in Figure 8 and Figure 9, respectively. It is observed from Figure 8 that at low frequencies, M' approached to zero at all temperatures under study indicating the suppression of the electrode polarization effect [58, 59]. In general, the M' increased with increase in frequency at each temperature and reaches the maximum value at high frequency, which is due to the presence of relaxation process [60]. It is also observed that the value of M' decreases with an increase of temperature. The M' of chitosan and Cs-20% γ-Fe_2O_3 increased with increase in frequency. The M' peak shifts to higher frequencies with increase in temperature up to 353K. Above 353K, it shifted to lower frequency. This is attributable to stiffening of the polymer due to evaporation of water present in the films. The M' of Cs-graphite and Cs-graphite-γ-Fe_2O_3 composites increased with increase of frequency at each temperature. At 1MHz, broad peak is observed and it decreased continuously with an increase of temperature. The reduction of M' with temperature is due to the increase in the mobility of the polymer segment and charge carriers. At high temperatures, the orientation of charge carriers and molecular dipoles become easier due to thermally activated process. Addition of γ-Fe_2O_3 nanoparticles into Cs-graphite composites enhanced the frequency independent behaviour of M' at low frequency and this long tail is attributed to the large capacitance associated with the accumulation of γ-Fe_2O_3 nanoparticles at the interface of Cs-graphite composites [61].

The frequency dependence of imaginary part of electric modulus (M'') is shown in Figure 9. At lower frequency, M″ exhibits very low value which is due to the large value of capacitance associated with the electrode polarization effect as a result of accumulation of a large amount of charge carriers at the sample/electrode interface [62]. However, at high frequencies well defined peaks were observed. M'' peak denotes the conductivity relaxation of the material. The asymmetric peak broadening of M'' suggest non-Deybe type of relaxation in the PNCs [63]. The frequency region below the M'' peak maximum indicates the long range hopping of the charge carriers, while region to the right side of the peak maximum indicates the short range hopping. The frequency range where the peak occurs is suggestive of the transition from long range to short range hopping. The relaxation peaks were shifted to high frequency with an increase of temperature. It indicates the reduction of relaxation time and enhancement of conductivity (by hopping of charge carriers) [64-65]. The M'' of Chitosan [Figure 9a] shows peak at ~ 7910 Hz (303K) and is shifted to high frequency with an increase of temperature up to ~28,380 Hz (353K). Similarly, the Cs-20% γ-Fe_2O_3 [Figure 9b] shows the peak at ~8315 Hz (303K) and it is shifted up to ~ 34,665 Hz (353K) with an increase of temperature. In between the temperature 363-423K, the M'' peaks of both the samples were shifted to low frequency side. It is attributable to the removal of water molecules from the films due to increase in temperature. When 10wt% of graphite is added in to the chitosan matrix, the intensity of M'' peak is reduced. The M'' of Cs-10% graphite [Figure 9c] shows peak at ~1144 Hz (303K) and it is shifted to high frequency with an increase of temperature up to ~30,677Hz (373K). After 383K, the peaks were shifted beyond the measurable frequency (1 MHz). When 20wt% of γ-Fe_2O_3 nanoparticles were added into the Cs-10% graphite, the intensity of M'' peaks were further reduced. Initially, the M'' peak of Cs-10% graphite-20%γ-Fe_2O_3 [Figure 9d] is observed at ~ 5135 Hz (303K) and it is shifted towards high frequency side with an increasing of

temperature up to ~95,486 Hz (363K). Above 363K, the peaks were shifted to beyond measurable frequency range.

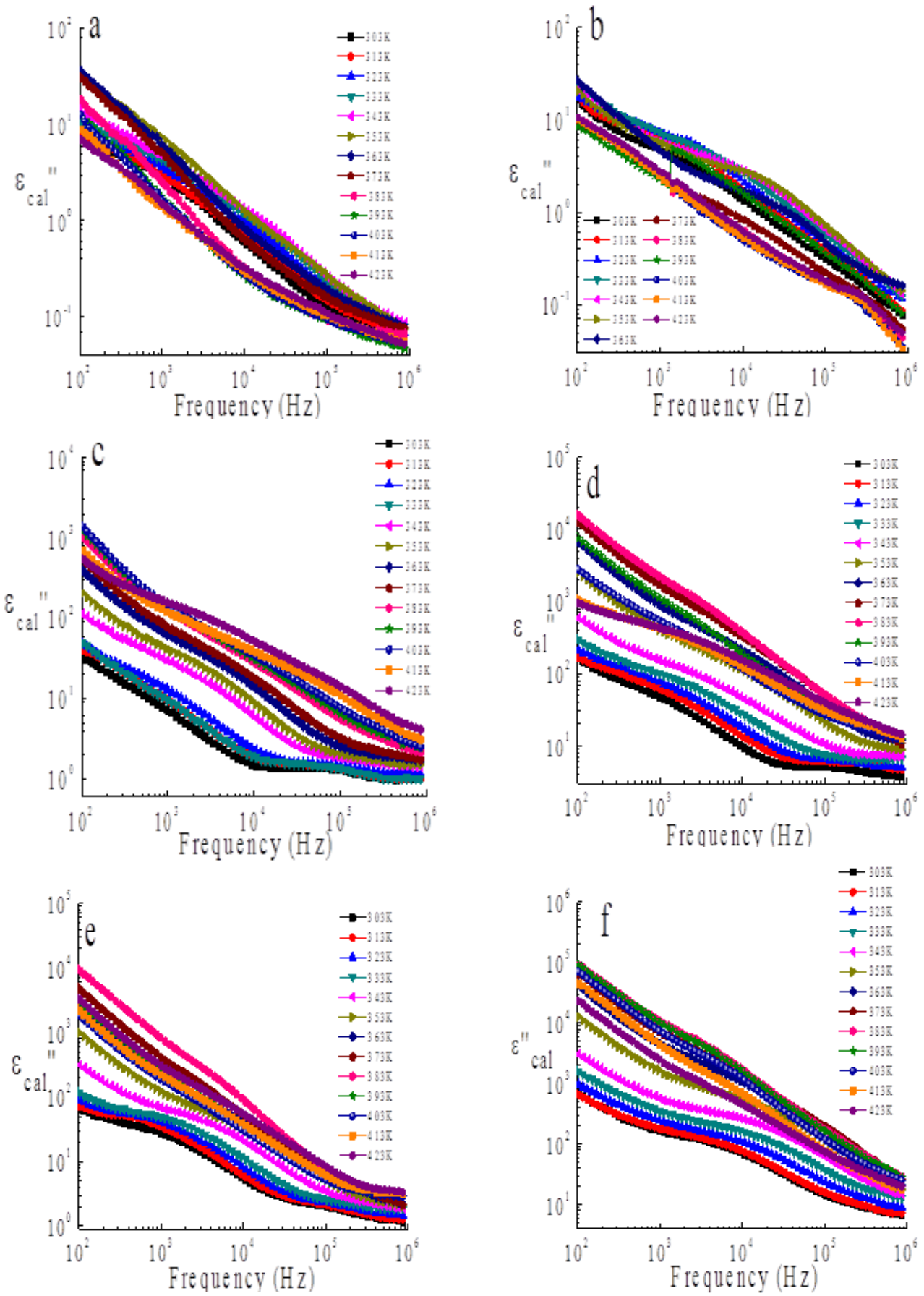

Fig. 7. Frequency dependent variation of dielectric loss (ε_{cal}'') at various temperature for a) Chitosan, b) Cs-20% γ-Fe_2O_3, c) Cs-10% graphite, d) Cs-10% graphite-20% γ-Fe_2O_3, e) Cs-20% graphite and f) Cs-20% graphite-20% γ-Fe_2O_3.

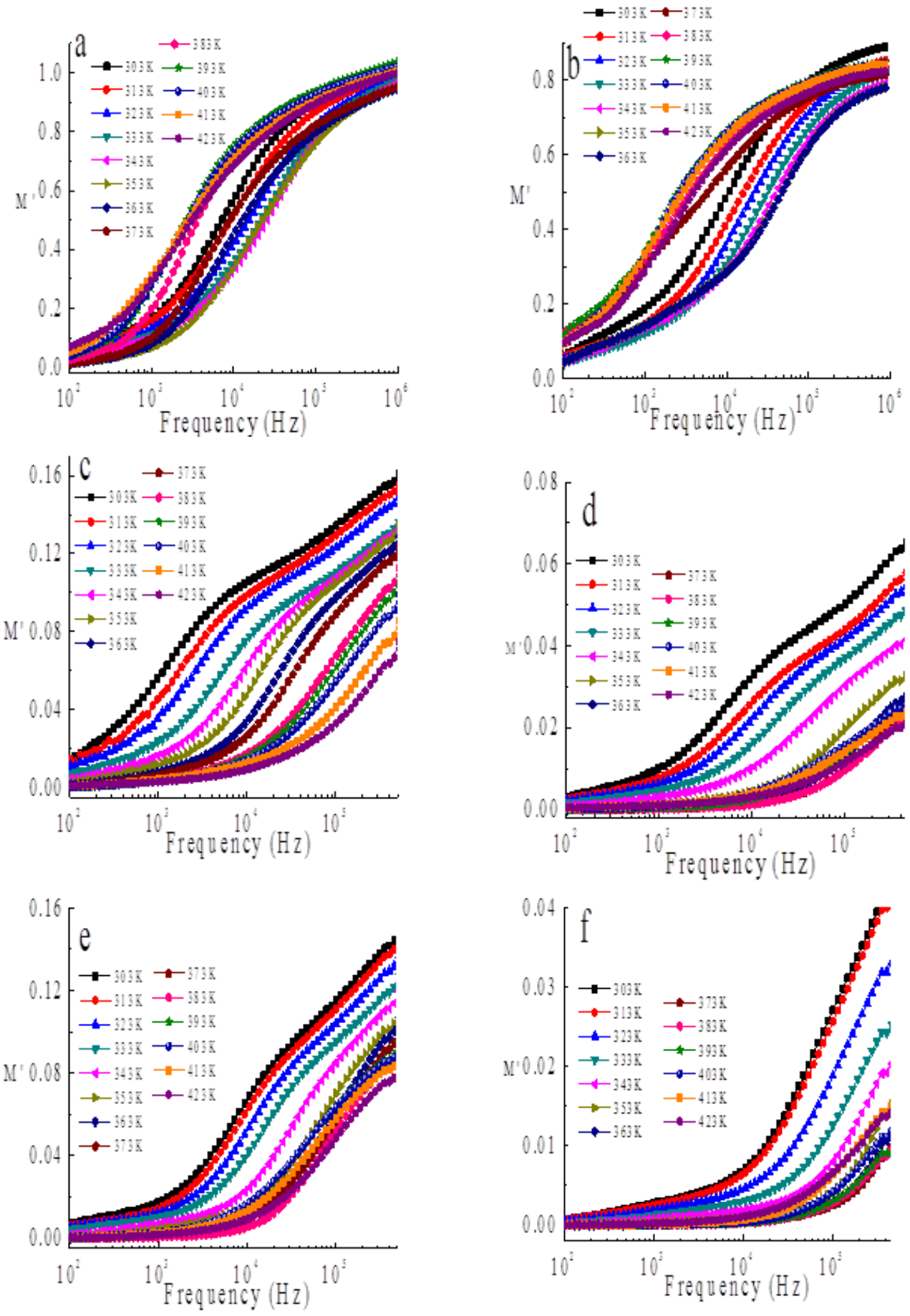

Fig. 8. Frequency dependent variation of real part of electric modulus (M') at various temperature for a) Chitosan, b) Cs-20% γ-Fe_2O_3, c) Cs-10% graphite, d) Cs-10% graphite-20% γ-Fe_2O_3, e) Cs-20% graphite and f) Cs-20% graphite-20% γ-Fe_2O_3.

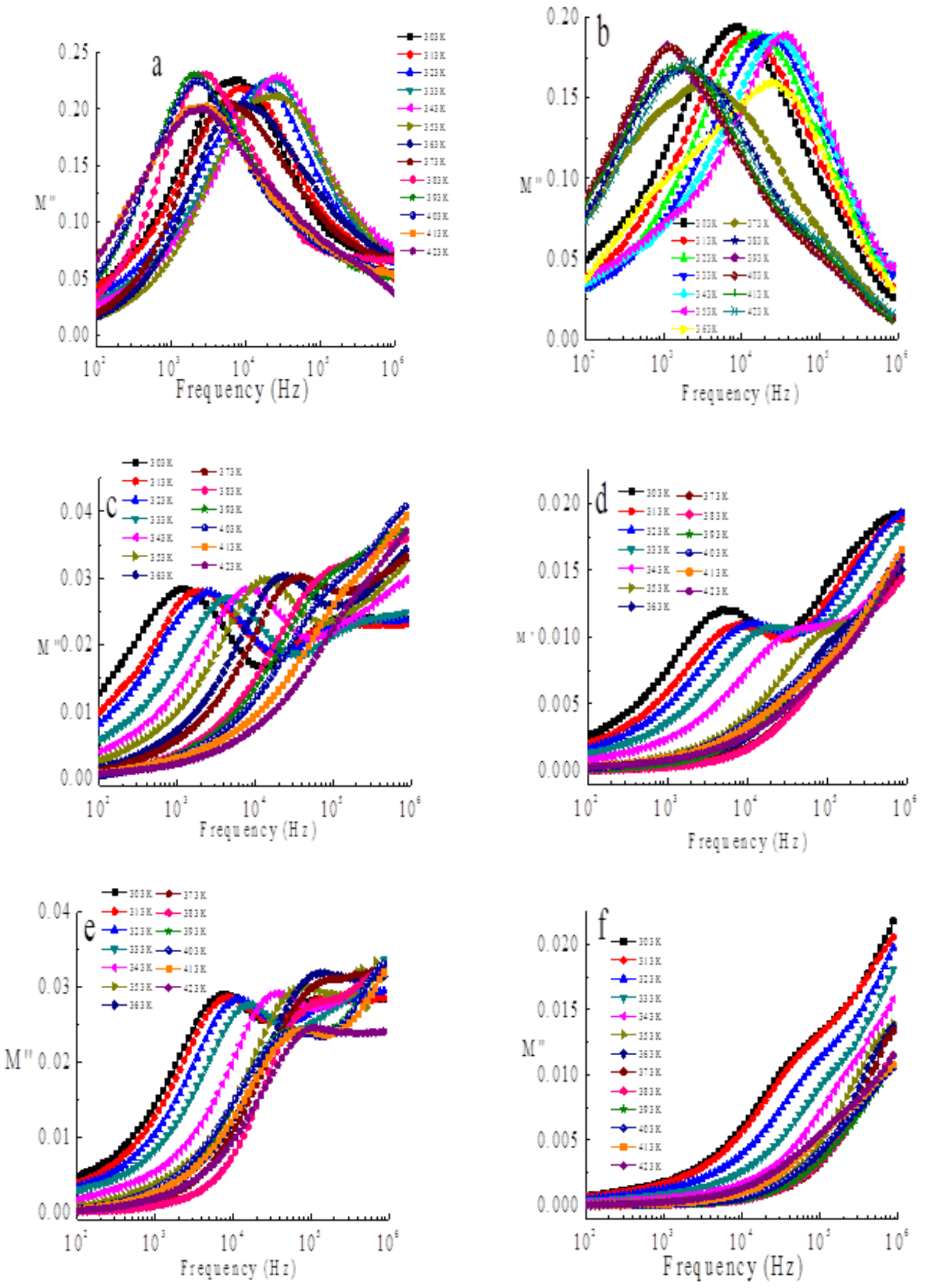

Fig. 9. Frequency dependent variation of imaginary part of electric modulus (M") at various temperature for a) Chitosan, b) Cs-20% γ-Fe_2O_3, c) Cs-10% graphite, d) Cs-10% graphite-20% γ-Fe_2O_3, e) Cs-20% graphite and f) Cs-20% graphite-20% γ-Fe_2O_3.

Increasing of graphite concentration from 10 to 20 wt%, resulted in the shifting of the M'' peaks to high frequency. The Cs-20% graphite [Figure 9e] has peak at ~ 7205 Hz (303K) and is shifted to high frequency with an increase of temperature up to ~ 1,58,247 Hz (373K). Above 373K, the peaks were shifted to low frequency. In between the temperature (393-423K), the M'' peaks were shifted from ~ 48,507 Hz (393K) to ~ 95,486 Hz (423K). Addition of 20wt% of γ-Fe_2O_3 nanoparticles into the Cs-20% graphite shifts the M'' peak towards high frequency side. The Cs-20% graphite-20% γ-Fe_2O_3 [Figure 9f] shows the mild peak at ~37,158 Hz (303K) and it is shifted to high frequency with an increase of temperature up to ~1,05,292 Hz (333K). Above 333K, peaks were shifted to beyond measurable frequency range. A combined study of electric modulus and permittivity formalism is used to distinguish localized dielectric relaxation phenomena from long range conductivity. A relaxation peak in the frequency spectra of the imaginary component M'' and no peak corresponding plot of ε" indicates the pure conduction process. However, peak appears both in M* and ε* representation denotes the dielectric relaxation process. In our work, peaks appeared only in the imaginary component of M and it indicates the pure conduction process associated with the material. This also suggests that ionic and polymer segmental motion is strongly coupled in the PNCs [66-68].

3.6.4. Frequency dependence of Dissipation factor (D)

Fig. 10 shows the frequency dependence of dissipation factor for chitosan and its PNCs at different temperature. The peaks shifted to high frequency with increase in temperature. At high temperature, it is shifted towards low frequency. Chitosan [Figure 10a] shows the peak at ~ 1478Hz (303K) and it is shifted to high frequency with an increase of temperature up to ~3296Hz (343K). In between the temperature (343-373K), it shifted to low frequency. Above 373K, no peak is observed. Addition of 20 wt% of γ-Fe_2O_3 nanoparticles into the chitosan films affected the dissipation factor. Cs-20% γ-Fe_2O_3 [Figure 10b] showed peak at ~ 2017 Hz (303K) and it shifted to high frequency with increase of temperature up to ~ 13619 Hz (353K). Above 353K, no peak was observed. Both chitosan and Cs-20% γ-Fe_2O_3 show very low dissipation value at 1 MHz. The dissipation factor of chitosan is affected by introduction of graphite. The Cs-10% graphite [Figure 10c] did not show any peak in the temperature range of 303-343K. Above 343K, it shows peak at ~150Hz (403K). Addition of 20 wt% of γ-Fe_2O_3 nanoparticles into the Cs-10% graphite induces new relaxation. The Cs-10%graphite-20%γ-Fe_2O_3 [Figure 10d] shows single peak in the temperature range of 303K to 343K, after that it shows a peaks in the temperature range of 353-403K. A relaxation peak is observed at ~1819 Hz (303K) and it is shifted to high frequency with an increase of temperature up to ~28,135 Hz (373K). On further increasing of temperature the peaks were suddenly shifted to low frequency at ~10,679 Hz (383K) and it is further decreased to ~7,027 Hz (403K) with an increase of temperature. Finally, peak is observed at ~21,369 (423K). When increasing the graphite concentration from 10 to 20 wt%, the low temperature relaxation peaks were clearly observed. The Cs-20% graphite [Figure 10e] shows the peak at ~2506 Hz (303K) and it is shifted to high frequency with increase of temperature up to ~ 17,901 Hz (353K). With further increase of the temperature, the relaxation peaks shifted to low frequency. At high temperature (423K), the relaxation peak is observed at ~269Hz. Addition of 20 wt% of γ-Fe_2O_3 nanoparticles in to the Cs-20% graphite also shows two relaxation peaks. The Cs-20%graphite-20%γ-Fe_2O_3 [Figure 10f] shows only one peak in the temperature range of 303-333K and two peaks in the temperature range of 343-423K. The first peak is shifted to high frequency with an increase of temperature up to ~422Hz (423K). The second peak is observed at ~15,107 Hz (303K) and it is shifted to high frequency with an increase of temperature up to ~ 30,228Hz (383K). Above 383K, it decreased to low frequency. At high temperature (423K), the peak is observed at ~1,946 Hz.

3.6.5. Electrical Conductivity

3.6.5. (a) Frequency dependence of electrical conductivity

The frequency dependence of ac electrical conductivity (σ_{ac}) for chitosan and the PNCs at different temperature is shown in Figure 11. At low frequency (100 Hz), the conductivity is constant which corresponds to the dc part of the conductivity. At higher frequencies, it shows dispersion. It is observed from the figure that the dc conductivity increases with increase in temperature. The conductivity dispersion in the sample is generally analyzed by using Jonscher power law [69]:

$$\sigma_{ac} = \sigma_{dc} + A\omega^n \quad (10)$$

Where σ_{dc} is the frequency independent conductivity, A is a temperature independent factor and n is the power law exponent which generally varies between 0 and 1. The exponent n represents the degree of interactions between the conducting species. It is observed that the σ_{ac} of all the samples slowly increases at low frequencies while at higher frequencies it increases rapidly. In particular frequency where the change in slope of the ac conductivity takes place is known as the critical frequency (f_c) which indicates that the sign of the change in the conductivity mechanisms from the long range to the short range conduction. It is observed that the critical frequency is temperature dependent and it shifts towards higher frequencies with an increase of temperature. The conductivity of chitosan is mainly due to motion of H^+ and acetate anions. The σ_{ac} of chitosan [Figure 11a] shows typical insulating behaviour with a frequency dependent conductivity and it increased linearly with frequency in the temperature range from 303K to 343K. Suddenly, frequency independent behaviour is observed at

low frequency side in the temperature range of 353K to 423K. Subsequently, it shows high value of σ at 363K. After that, the σ decreased with further increase of temperature up to 423K. The σ_{ac} of chitosan is enhanced by inclusion of γ-Fe_2O_3 nanoparticles and graphite. When 20 wt% of γ-Fe_2O_3 nanoparticles were added into chitosan, its conductivity is enhanced slightly. The σ_{ac} of Cs-20%γ-Fe_2O_3 [Figure 11b] increased with increase in frequency and it increased up to 363K, after that it is decreases with further increase of temperature. When 10 wt% of graphite is added into chitosan, the conductivity is increased. The σ_{ac} of Cs-10% graphite [Figure 11c] increased with increase in frequency and it is increased with increase in temperature up to 403K and after that it decreased. The continuous increase of conductivity up to 403K is due to the high thermal conductivity of graphite. When 20 wt% of γ-Fe_2O_3 nanoparticles is added to the Cs-10% graphite, the σ_{ac} of Cs-graphite is increased by one order of magnitude at room temperature. The σ_{ac} of Cs-10% graphite-20% γ-Fe_2O_3 [Figure 11d] gradually increases with increase in frequency. It also increases with increase in temperature up to 383K. Above 383K the conductivity decreases with further increase of temperature up to 423K. Increasing the graphite concentration from 10 to 20wt% in the chitosan matrix, increases its conductivity. The σ_{ac} of Cs–20% graphite [Figure 11e] increased with increase in frequency and it also increased with increase in temperature up to 383K. When 20 wt% of γ-Fe_2O_3 nanoparticles is added into the Cs-20% graphite, its conductivity is enhanced by nearly one order of magnitude at room temperature. The σ_{ac} of Cs-20% graphite-20%γ-Fe_2O_3 [Figure 11f] increased gradually with an increase in frequency and it also increased with increase in temperature up to 383K, after that it decreased with further increase of temperature. The sudden decrease in σ_{ac} at high temperature (373 - 423K) is due to removal of water molecules from the samples. Hence, the conductivity of chitosan is increased with addition of graphite and γ-Fe_2O_3 nanoparticles. The conductivity of Cs-graphite composites is increased by nearly one order of magnitude with addition of γ-Fe_2O_3 nanoparticles.

3.6.5 (b) Temperature dependence of electrical conductivity (ln σ vs 1000/T)

The temperature dependence of dc electrical conductivity for the chitosan film and the PNCs are shown in Figure 12. The plot shows that as temperature increases, the σ_{dc} for all the samples increased up to 383K. It is due to increase in the drift mobility of the thermally activated charge carriers. After that, the σ_{dc} decreased with further increase of temperature. The sudden decrease of conductivity is due to the removal of water molecules from the sample. It is also observed that the σ_{dc} of Cs-graphite is enhanced with addition of γ-Fe_2O_3 nanoparticles. The σ_{dc} for all the samples increases from room temperature to 343K, indicating an Arrhenius type conductivity. One of the important parameter obtained from the above analysis is the activation energy (E_a). This is the energy required for the charge carriers to move inside the material and it is evaluated from the following equation

$$\sigma_{dc} = \sigma_o \exp(-E_a/\kappa T) \quad (11)$$

Where σ_{dc} is the conductivity at particular temperature, σ_o is pre-exponential factor, k is the Boltzmann's constant and T is the absolute temperature. The activation energy was calculated from the slope of the straight line obtained from ln σ *vs*1000/T. The regression values R^2 lies in 0.91–0.99, confirming all the points lie more or less in a straight line. The conductivity and activation energy of the materials are inversely proportional to each other [70]. The activation energy and σ_{dc} at room temperature for all the samples are listed in table 3. The activation energy (E_a) for the chitosan is found to be 36.5 kJ/mol. The activation energy decreased with an addition of γ-Fe_2O_3 nanoparticles or graphite. The E_a of Cs-graphite is decreased with an addition of γ-Fe_2O_3 nanoparticles. At the same time its conductivity is increased with addition of γ-Fe_2O_3 nanoparticles.

3.7. Magnetic measurement studies

Magnetic nature of the samples at room temperature was investigated by using SQUID - VSM with applied magnetic field sweeping from -70 kOe to +70 kOe [Figure 13]. The M-H curve of γ-Fe_2O_3 nanoparticles and the PNCs shows zero coercivity and zero retenivity, that is, there is no hysteresis in the magnetization curve [Figure 13 (a,b)]. It indicates the superparamagnetic behaviour [19].The saturation magnetization of γ-Fe_2O_3 nanoparticles (33 emu/g) is lower than the reported bulk maghemite value (76 emu/g) [71]. It could be because of size of γ-Fe_2O_3 nanoparticles [d_{XRD} = 14nm] [72]. The M-H curve of chitosan shows diamagnetic behaviour with a room temperature magnetization of 0.0178 emu/g [inset of Figure 13 (a)]. Subtracting the diamagnetic contribution from the chitosan film, the saturation magnetization of Cs-20%γ-Fe_2O_3, Cs-10%graphite-20%γ-Fe_2O_3 and Cs-20%graphite-20%γ-Fe_2O_3 was found to be 4.18 emu/g, 2.83 emu/g and 3.17 emu/g, respectively. The saturation magnetization of polymer nanocomposites was found to be less than that of the γ-Fe_2O_3 nanoparticles (33emu/g). This superparamagnetic behaviour of the nanocomposites suggests the uniform distribution of magnetic nanoparticles in to the chitosan matrix.

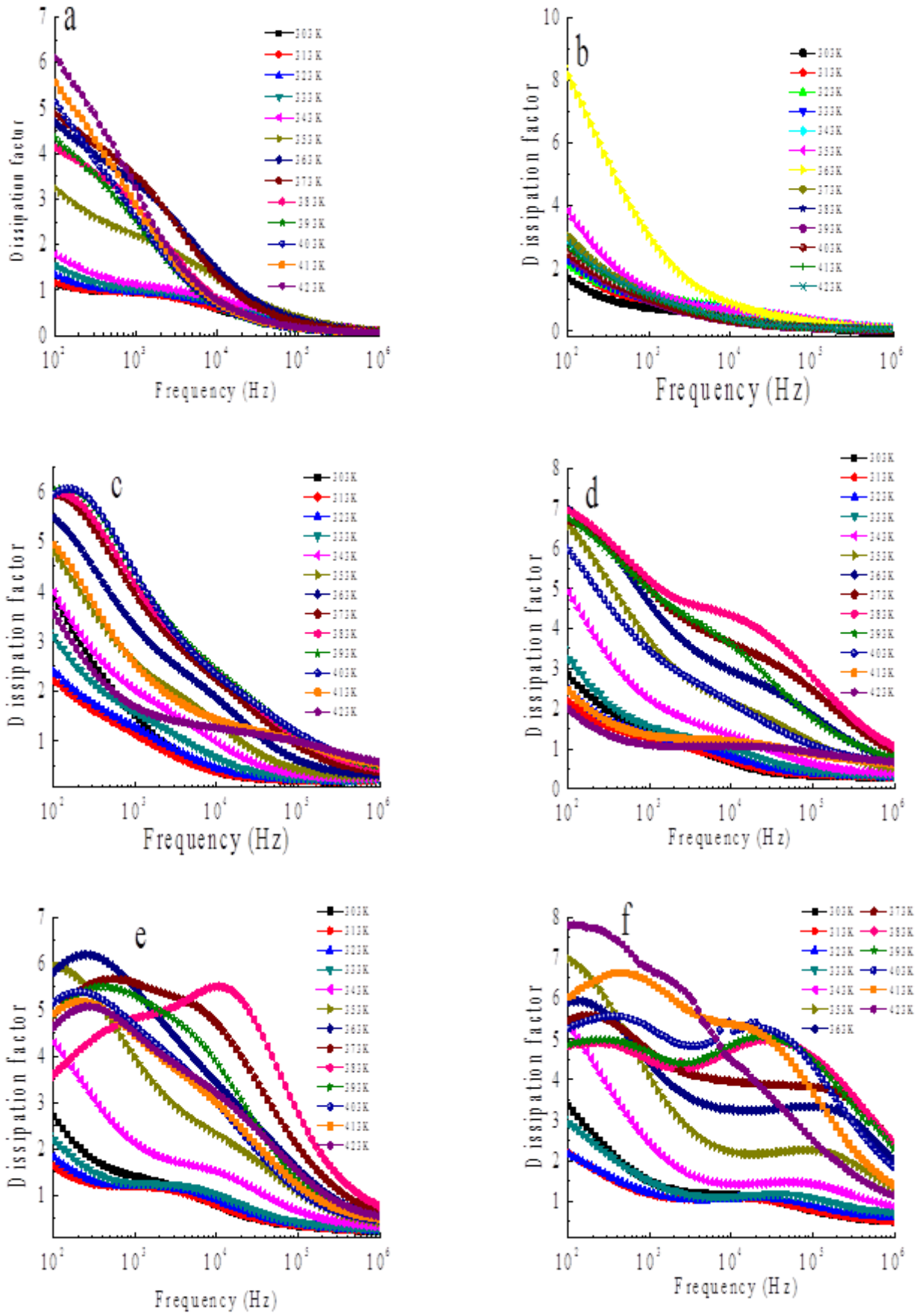

Fig. 10. Frequency dependent variation of dissipation factor at various temperature for a) Chitosan, b) Cs-20% γ-Fe_2O_3, c) Cs-10% graphite, d) Cs-10% graphite-20% γ-Fe_2O_3, e) Cs-20% graphite and f) Cs-20% graphite-20% γ-Fe_2O_3.

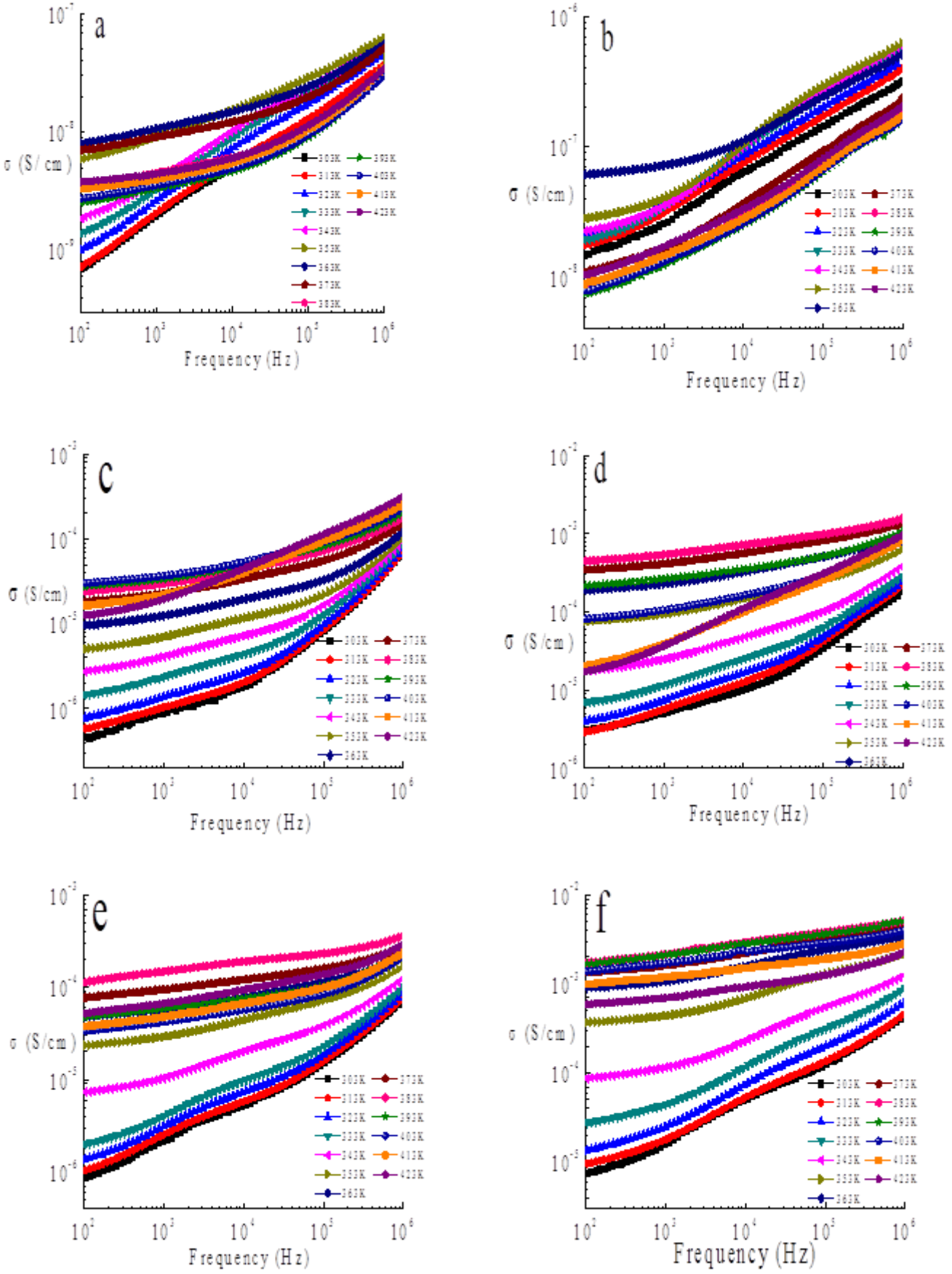

Fig. 11. Frequency dependent variation of electrical conductivity at various temperature for a) chitosan, b) Cs-20% γ-Fe_2O_3, c) Cs-10% graphite, d) Cs-10% graphite-20% γ-Fe_2O_3, e) Cs-20% graphite and f) Cs-20% graphite-20% γ-Fe_2O_3.

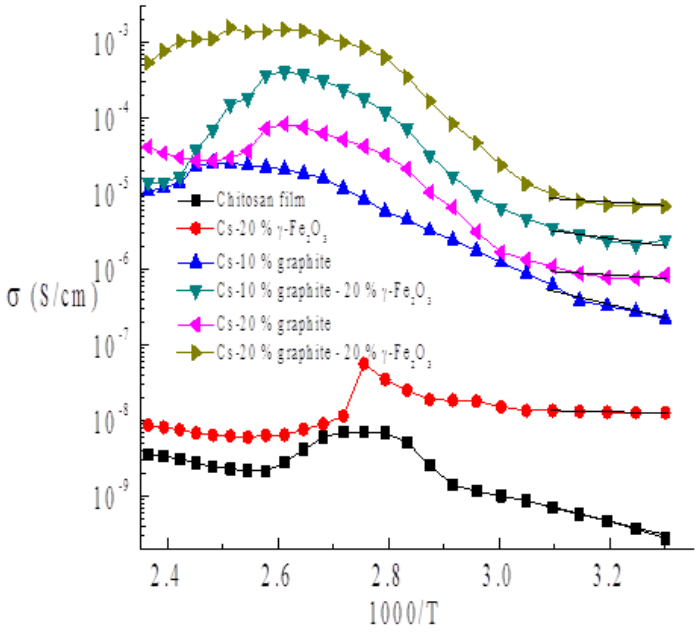

Fig.12. Arrhenius plot for dc electrical conductivity for chitosan and its PNCs.

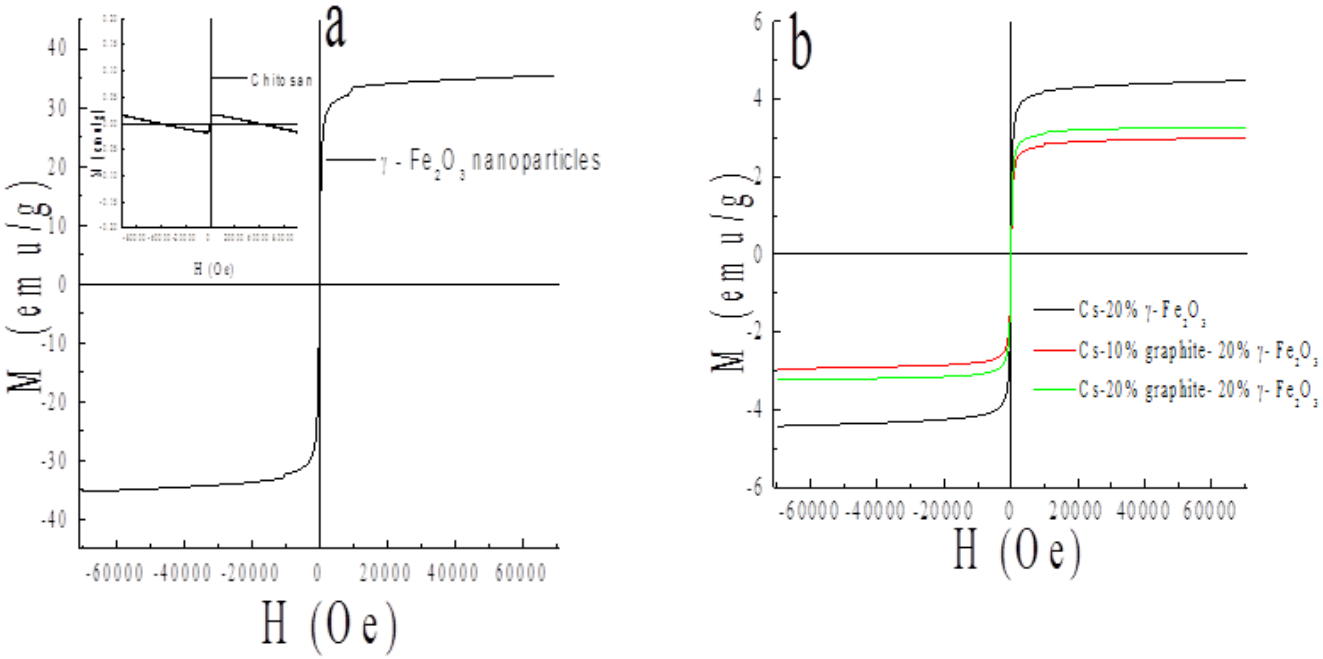

Fig.13. Room temperature M-H curve for a) γ-Fe_2O_3 nanoparticles and Chitosan film (insect); b) Polymer nanocomposite films.

Table 3. Activation energy and DC conductivity values for chitosan and its PNCs.

S.No	Sample	Ea (kJ/mol) (303K-343K)	σ_{dc} (S/cm)
1.	Chitosan	36.50	$2.5x10^{-10}$
2.	Cs-20% γ-Fe_2O_3	17.50	$1.2 x10^{-8}$
3.	Cs-10% graphite	27.93	$3.3 x10^{-7}$
4.	Cs-10% graphite-20% γ-Fe_2O_3	25.69	$2.5 x10^{-6}$
5.	Cs-20% graphite	20.95	$6.4 x10^{-7}$
6.	Cs-20% graphite-20% γ-Fe_2O_3	19.98	$5.8 x10^{-6}$

3.8. Model

The dielectric behaviour of the PNCs can be explained by the simple model as shown in Figure 14. When Chitosan is cast as films, it has crystallites. When graphene is incorporated in the films the crystallinity of the chitosan increases (Figure 14 A) (the chitosan units are shown to be assembled in an orderly manner). The crystallinity of the chitosan films decreases with the incorporation of maghemite (Figure 14 B). The dielectric constant increases when the concentration of graphite is increased in it. The dielectric constant further increases with incorporation of maghemite in the films. The dielectric constant of the chitosan-maghemite-graphite films is greater than the sum of the dielectric constant of the chitosan – maghemite films and chitosan –graphite films. Chitosan-maghemite-graphite films become high dielectric constant materials when the maghemite concentration is 20%. This drastic increase in the dielectric constant can be due to formation of micro capacitors in the nanocomposites (Figure 14 C). These microcapacitors are formed by the trapping of maghemite nanoparticles between tow graphites (shown as red circle in Figure 14C). As a result, the capacitance increases giving rise to higher dielectric constant values. Also, the conductivity increases with increase in temperature. The activation energy decreases with increase in graphite concentration and it further decreases with incorporation of 20% γ-Fe_2O_3 in the films. The conductivity increases as graphite concentration increases and it is further increased by about 10 times due to incorporation of 20% γ-Fe_2O_3 in the films. This indicates that maghemite increases hopping of the charges in the films.

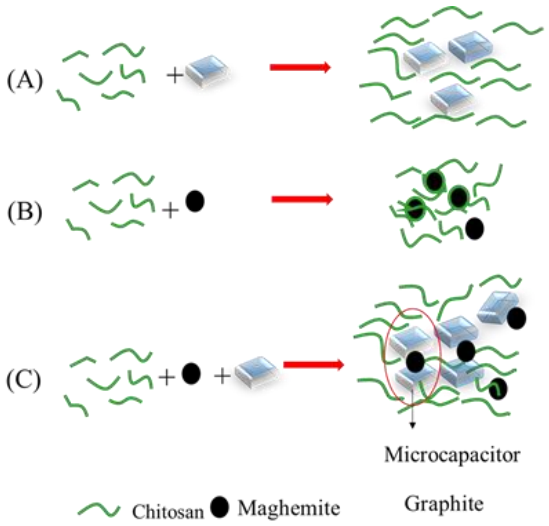

Fig.14. Model for formation of microcapacitor in the polymer nanocomposites.

4. Conclusion

PNCs of chitosan containing graphite and γ-Fe_2O_3 nanoparticles were prepared by solution casting method. The XRD and Raman result revealed the incorporation of graphite and γ-Fe_2O_3 nanoparticles into the chitosan matrix. The crystallinity of chitosan films were increased by the incorporation of graphite and it decreased due to incorporation of maghemite. The dielectric constant increased due to addition of graphite and it further increased due to further addition of γ-Fe_2O_3 nanoparticles in the chitosan films. The conductivity also showed a similar trend. The presence of graphite with γ-Fe_2O_3 reduced the activation energy and increased hopping of charges leading to increase in the electrical conductivity of the PNCs. All the PNCs with γ-Fe_2O_3 retained their superparamagnetic features like pure maghemite. Hence, it can be concluded that Cs-graphite-γ-Fe_2O_3 nanocomposites is a superparamagnetic, flexible and capacitance tuneable nanocomposite comprising of microcapacitors. This research could benefit research in batteries.

Acknowledgement

The research was made possible due to funding provided by BOARD OF RESEARCH IN NUCLEAR SCIENCES (BRNS) India Sanction No 2011/37C/21/BRNS.

References

1. G. Landi, A. Sorrentino, F. Fedi, H.C. Neitzert, S. Iannace, "Cycle stability and dielectric properties of a new biodegradable energy storage material." Nano Energy 17 (2015) 348-355.
2. Z. Yue, I. J. McEwen, J.M.G. Cowie, "Novel gel polymer electrolytes based on a cellulose ester with PEO side chains." Solid State Ionics 156 (2003) 155-162.
3. S. Ramesh, C.W. Liew, A.K. Arof, "Ion conducting corn starch biopolymer electrolytes doped with ionic liquid 1-butyl-3-methylimidazolium hexafluorophosphate." Journal of Non-Crystalline Solids 357 (2011) 3654-3660.
4. A.S.A. Khair, R. Puteh, A.K. Arof, "Conductivity studies of a chitosan-based polymer electrolyte." Physica B 373 (2006) 23-27.
5. K. Pandiselvi, S. Thambidurai, "Chitosan-ZnO/polyaniline ternary nanocomposite for high-performance supercapacitor." Ionics 20 (2013) 551-561.
6. V.K. Mourya, N.N. Inamdar, "Chitosan-modifications and applications: Opportunities galore." React Funct Polym 68 (2008) 1013-1051.
7. M. Dash, F. Chiellini, R.M. Ottenbrite, E.Chiellini, "Chitosan-A versatile semi-synthetic polymer in biomedical applications." Progress in Polymer Science 36 (2011) 981-1014.
8. S.N. Suraiya Begum, V.K. Aswal, R.P. Ramasamy, "Chitosan–Gold–Lithium Nanocomposites as Solid Polymer Electrolyte." Journal of Nanoscience and Nanotechnology 14 (2014) 1-13.
9. J. B. Gonzalez-Campos, E. Prokhorov, G. Luna-Barcenas, I. C. Sanchez, J. Lara-Romero, M. E. Mendoza-Duarte, F. Villasenor, L. Guevara-Olvera, "Chitosan/Silver Nanoparticles Composite: Molecular Relaxations Investigation by Dynamic Mechanical Analysis and Impedance Spectroscopy." Journal of Polymer Science Part B: Polymer Physics 48 (2010) 739-748.
10. S.R. Majid, A.K. Arof, "Electrical behavior of proton-conducting chitosan-phosphoric acid-based electrolytes." Physica B 390 (2007) 209-215.
11. P. Agrawal, G.J. Strijkers, K. Nicolay, "Chitosan-based systems for molecular imaging." Advanced Drug Delivery Reviews 62 (2009) 42-58.
12. P. Mukoma, B.R. Jooste, H.C.M.J. Vosloo, "Synthesis and characterization of cross-linked chitosan membranes for application as alternative proton exchange membrane materials in fuel cells." Journal Power Sources 136 (2004) 16-23.
13. L. Chai, Q. Qu, L. Zhang, M. Shen, L. Zhang, H. Zheng, "Chitosan, a new and environmental benign electrode binder for use with graphite anode in lithium-ion batteries." Electrochimica Acta 105 (2013) 378-383.
14. Mohammad Hemmati, Majid Jafar Tafreshi, Mohammad Hossein Ehsani, Sanaz Alamdari, "Highly sensitive and wide-range flexible sensor based on hybrid BaWO4@CS nanocomposite." Ceramics International 48 (2022) 26508–26518]
15. K. Kalaitzidou, H. Fukushima, L.T. Drzal, "Multifunctional polypropylene composites produced by incorporation of exfoliated graphite nanoplatelets." Carbon 45 (2007) 1446-1452.
16. A. Celzardt, E. McRae, J.F. Mareche, "Composites based on micron-sized exfoliated graphite particles: Electrical conduction critical exponents and anisotropy." Journal Physics Chemistry Solids 57 (1996) 715-718.
17. S. Stankovich, D.A. Dikin, G.H.B. Dommett, K.M. Kohlhaas, E.J. Zimney, R.C. Piner, S.T.N guyen, R.S. Ruoff, "Graphene-based composite materials." Nature 442 (2006) 282-286.
18. H. Kaczmarek, A. Podgorski, "Photochemical and thermal behaviours of poly (vinyl alcohol)/graphite oxide composites." Polymer Degradation and Stability 92 (2007) 939-946.
19. A.H. Lu, E. L. Salabas, F. Schuth, "Magnetic Nanoparticles: Synthesis, Protection, Functionalization, and Application." Angewandte Chemie International Edition 46 (2007) 1222-1244.
20. S. Laurent, D. Forge, M. Port, A. Roch, C. Robic, L. V. Elst, R. N. Muller, "Magnetic Iron Oxide Nanoparticles: Synthesis, Stabilization, Vectorization, Physicochemical Characterizations, and Biological Applications." Chemical Reviews 108 (2008) 2064-2110.
21. E. Mitchell, R.K. Gupta, K.M. Darkwa, D. Kumar, K. Ramasamy, B.K. Gupta, P. Kahol, "Facile synthesis and morphogenesis of superparamagnetic iron oxide nanoparticles for high-performance supercapacitor applications." New Journal of Chemistry 38 (2014) 4344-4350.
22. P. Luo, J. Yu, Z. Shi, F. Wang, L. Liu, H. Huang, Y. Zhao, H. Wang, G. Li, Y. Zou, "Fabrication and supercapacitive properties of Fe_2O_3@C nanocomposites." Materials Letters 80 (2012) 121-123.

23. B. Natesan, N.K. Karan, R.S. Katiyar, "Ion relaxation dynamics and nearly constant loss behavior in polymer electrolyte." Physical Review E 48 (2006) 042801-042805.
24. S.J. Lee, J.R. Jeong, S. C. Shin, J.C. Kim, J.D. Kim, "Synthesis and characterization of superparamagnetic maghemite nanoparticles prepared by coprecipitation technique." Journal of Magnetism and Magnetic Materials 282 (2004) 147–150.
25. G.H. Podrepsek, Z. Knez, "Different preparation methods and characterization of magnetic maghemite coated with chitosan." Journal of Nanoparticle Research 15 (2013) 1751-1763.
26. S.F. Wang, L. Shen, W.D. Zhang, "Preparation and Mechanical Properties of Chitosan/Carbon Nanotubes Composites." Biomacromolecules 6 (2005) 3067–3072.
27. K. Rudzka, A.V. Delgado, J.L. Viota, "Maghemite Functionalization for Antitumor Drug Vehiculization." Molecolar Pharmaceutics 9 (2012) 2017–2028.
28. N. Valinezhad, A. F. Talebi, S. Alamdari, Biosynthesize, "physicochemical characterization and biological investigations of chitosan-Ferula gummosa essential oil (CS-FEO) nanocomposite." International Journal of Biological Macromolecules 241 (2023) 124503.
29. J. Chen, J. Xu, K. Wang, X. Qian, R. Sun, "Highly Thermostable, Flexible, and Conductive Films Prepared from Cellulose, Graphite, and Polypyrrole Nanoparticles." ACS Applied Materials & Interfaces 7 (2015) 15641-15648.
30. C. Peniche, W. Argüelles-Monal, N. Davidenko, R. Sastre, A. Gallardo J. San Román, "Self-Curing Membranes of Chitosan/PAA IPNS Obtained by Radical Polymerization: Preparation, Characterization and Interpolymer Complexation." Biomaterials 20 (1999) 1869–1878.
31. Y. Ge, Y. Zhang, J. Xia, M. Ma, S. He, F. Nie & N. Gu, "Effect of surface charge and agglomerate degree of magnetic iron oxide nanoparticles on KB cellular uptake in vitro." Colloids and Surfaces B: Biointerfaces, 73(2009) 294–301.
32. Z. Liu, L. Jiang, F. Galli, I. Nederlof, R. C. L. Olsthoorn, G.E.M. Lamers, T. H. Oosterkamp & J. P. Abrahams, "A graphene oxide streptavidin complex for biorecognition–towards affinity purification." Advanced Functional Materials, 20 (2010) 2857–2865.
33. Z.L. Chen, F.Y. Kam, R.G.S. Goh, J. Song, G. K. Lim & L.L. Chua, "Influence of Graphite Source on Chemical Oxidative Reactivity'." Chemistry of Materials 25 (2013) 2944–2949.
34. J. Gu, X. Yang, Z. Lv, N. Li, C. Liang & Q. Zhang, "Functionalized graphite nanoplatelets/epoxy resin nanocomposites with high thermal conductivity." International Journal of Heat and Mass Transfer 92 (2016) 15–22.
35. R.I. Jibrael, M.K.A. Mohammed, "Production of graphene powder by electrochemical exfoliation of graphite electrodes immersed in aqueous solution." Optik 127 6384–6389.
36. A.R. Futyra, M. Kus-Liskiewicz, V. Sebastian, S. Irusta, M. Arruebo, G. Stochel, A. Kyzioł, "Development of Noncytotoxic Chitosan–Gold nanocomposites as Efficient Antibacterial Materials." ACS Applied Materials and Interfaces 7 (2015) 1087–1099.
37. M. Yadav, K.Y. Rhee, S. J. Park & D. Hui, "Mechanical properties of Fe_3O_4/GO/chitosan composites." Composites Part B 66 (2014) 89–96.
38. K. J. Lee, J. H. An, J.S. Shin, D. H. Kim, C. Kim, H. Ozaki, J. G. Koh, "Protective effect of maghemite nanoparticles on ultraviolet-induced photo-damage in human skin fibroblasts." Nanotechnology 18 (2007) 465201-465207.
39. L. Kong, X. Yin, Y. Zhang, X. Yuan, Q. Li, F. Ye, L. Cheng, L. Zhang, "Electromagnetic Wave Absorption Properties of Reduced Graphene Oxide Modified by Maghemite Colloidal Nanoparticle Clusters." The Journal of Physical Chemistry C 117 (2013) 19701- 19711.
40. A. C. Ferrari, D. M. Basko, "Raman spectroscopy as a versatile tool for studying the properties of graphene." Nature Nanotechnology 8 (2013) 235-246.
41. J. Jagiello, J. Judek, M. Zdrojek, M. Aksienionek, L. Lipinska, "Production of graphene composite by direct graphite exfoliation with chitosan." Materials Chemistry and Physics 148 (2014) 507-511.
42. A. Janes, H. Kurig, E. Lust, "Characterisation of activated nanoporous carbon for supercapacitor electrode materials." Carbon 45 (2007) 1226-1233.
43. A. Reina, X. Jia, J. Ho, D. Nezich, H. Son, V. Bulovic, M.S. Dresselhaus, J. Kong, "Large Area, Few-Layer Graphene Films on Arbitrary Substrates by Chemical Vapor Deposition." Nano Letters 9 (2008) 30–35.
44. A.C. Ferrari, J. Robertson, "Interpretation of Raman spectra of disordered and amorphous carbon." Physical Review B 61 (2000) 14095-14107.
45. M. Cheng, R. Yang, L.C. Zhang, Z.W. Shi, W. Yang, D.M. Wang, G.B. Xie, D.X. Shi, G.Y. Zhang, "Restoration of graphene from graphene oxide by defect repair." Carbon 50 (2012) 2581-2587.
46. L.G. Cancado, M.A. Pimenta, B.R.A. Neves, M.S.S. Dantas, A. Jorio, "Influence of the Atomic Structure on the Raman Spectra of Graphite Edges." Physical Review Letters 93 (2004) 247401.
47. S. Marland, A. Merchant, N. Rowson, "Dielectric properties of coal." Fuel 80 (2001) 1839-1849.
48. M. Markov, E. Kazatchenko, A. Mousatov, E. Pervago, "The dielectric permittivity of carbonate formations from the unified microstructure model." Journal of Applied Geophysics 76 (2012) 56-63.
49. A.L.M. Smits, M. Wubbenhorst, P.H. Kruiskamp, J.J.G. Van Soest, J.F.G. Vliegenthart, J. Van Turnhout, "Structure Evolution in Amylopectin/Ethylene Glycol Mixtures by H-bond Formation and Phase Separation Studied with Dielectric Relaxation Spectroscopy." The Journal of Physical Chemistry B 105 (2001) 5630-5636.
50. J. Wang, K. Zhao, "Dielectric analysis of chitosan–iron composite microspheres suspensions: Access to internal and interface electrokinetic information of microspheres." Colloids and Surfaces A: Physicochemical and Engineering Aspects 396 (2012) 270-277.
51. N.T. Tunga, T.V. Khai, H. Lee, D. Sohn, "The effects of dopant on morphology formation in polyaniline

graphite nanoplatelet composite." Synthetic Metals 161 (2011) 177-182.
52. J. Zhu, S. Wei, L. Zhang, Y. Mao, J. Ryu, N. Haldolaarachchige, D.P. Young, Z. Guo, "Electrical and dielectric properties of polyaniline–Al_2O_3 nanocomposites derived from various Al_2O_3 nanostructures." Journal of Materials Chemistry 21 (2011) 3952–3959.
53. A.S Bhatt, D. K. Bhat, M.S. Santosh, C.W Tai, "Chitosan/NiO nanocomposites: a potential new dielectric material." Journal of Materials Chemistry 21 (2011) 13490-13497.
54. X. Qian, N. Gu, Z. Cheng, X. Yang, E. Wang, S. Dong, "Impedance study of $(PEO)_{10}$ $LiClO_4$–Al_2O_3composite polymer electrolyte with blocking electrodes." Electrochimica Acta 46 (2001) 1829-1836.
55. M.M. El-Nahass, H.A.M. Ali, "AC conductivity and dielectric behavior of bulk Furfurylidenemalononitrile." Solid State Communications152 (2012) 1084-1088.
56. A. Molak, M. Paluch, S. Pawlus, J. Klimontko, Z. Ujma, I. Gruszka, "Electric modulus approach to the analysis of electric relaxation in highly conducting $(Na_{0.75}Bi_{0.25})(Mn_{0.25}Nb_{0.75})O_3$ ceramics." Journal of Physics D: Applied Physics 38 (2005) 1450-1460.
57. M.D. Migahed, M. Ishra, T. Fahmy. A. Barakat, "Electric modulus and AC conductivity studies in conducting PPy composite films at low temperature." Journal of Physics and Chemistry of Solids 65 (2004) 1121-1125.
58. F. Yakuphanoglu, "Electrical conductivity and electrical modulus properties of α, ω-dihexylsexithiophene organic semiconductor." Physica B 393 (2007) 139-142.
59. A. Dutta, T.P. Sinha, P. Jena, S. Adak, "Ac conductivity and dielectric relaxation in ionically conducting soda–lime–silicate glasses." Journal of Non-Crystalline Solids 354 (2008) 3952-3957.
60. L.N. Patro, K. Hariharan, "AC conductivity and scaling studies of polycrystalline SnF_2." Materials Chemistry and Physics 116 (2009) 81-87.
61. H.J. Woo, S.R. Majid, A.K. Arof, "Dielectric properties and morphology of polymer electrolyte based on poly(ε-caprolactone) and ammonium thiocyanate." Materials Chemistry and Physics 134 (2012) 755-761.
62. L.N. Patro, K. Hariharan, "Frequency dependent conduction characteristics of mechanochemically synthesized $NaSn_2F_5$." Materials Science and Engineering: B 162 (2009) 173-178.
63. M. Ram, S. Chakrabarti, "Dielectric and modulus studies on $LiFe_{1/2}Co_{1/2}VO_4$." Journal of Alloys and Compounds 462 (2008) 214-219.
64. M.Z.A. Yahya, A.K. Arof, "Conductivity and X-ray photoelectron studies on lithium acetate doped chitosan films." Carbohydrate Polymers 55 (2004) 95-100.
65. G.K. Moats, T.R. Noel, R.Parker, S.G. Ring, "Dynamic mechanical and dielectric characterisation of amylose–glycerol films." Carbohydrate Polymers 44 (2001) 247-253.
66. I.M. Hodge, M.D. Ingram, A.R. West, "Impedance and modulus spectroscopy of polycrystalline solid electrolytes." Journal of Electroanalytical Chemistry 74 (1976) 125-143.
67. R.Gerhardt, "Impedance and dielectric spectroscopy revisited: Distinguishing localized relaxation from long-range conductivity." Journal of Physics and Chemistry of Solids 55 (1994) 1491–1506.
68. P. Jevanandam, S. Vasudevan, "Arrhenius and non-Arrhenius conductivities in intercalated polymer electrolytes." The Journal of Chemical Physics 109 (1998) 8109.
69. A. Rouahi, A. Kahouli, A. Sylvestre, B. Yangui, "Impedance spectroscopic and dielectric analysis of $Ba_{0.7}Sr_{0.3}TiO_3$ thin films." Journal of Alloys and Compounds 529 (2012) 84-88.
70. M.A. Ahmed, M.A. El Hiti, M.K. El Nimr, M.A. Amer, "The ac electrical conductivity for Co-substituted SbNi ferrites." Journal of Magnetism and Magnetic Materials 152 (1996) 391-395.
71. A. Millan, A. Urtizberea, N.J.O. Silva, F. Palacio, V.S. Amaral, E. Snoeck, V. Serin, "Surface effects in maghemite nanoparticles." Journal of Magnetism and Magnetic Materials 312 (2007) L5–L9.
72. M. Rozman, M. Drofenik, "Hydrothermal Synthesis of Manganese Zinc Ferrites." Journal of the American Ceramic Society 78 (1995) 2449-2455.